Journal of Thermal Analysis and Calorimetry, Vol. 96 (2009) 2, 407–412

THERMAL CHARACTERIZATION OF A SPANISH RED MUD

J. Pascual[1], *F. A. Corpas*[2], *J. López-Beceiro*[3], *M. Benítez-Guerrero*[1] *and R. Artiaga*[3,*]

[1]Departamento de Ingeniería Civil, de Materiales y Fabricación. Universidad de Málaga
[2]Departamento de Ingeniería Química, Ambiental y de los Materiales. Universidad de Jaén
[3]Departamento de Ingeniería Industrial II. Universidad de A Coruña

A Spanish red mud was thermally characterized. Chemical and mineralogical composition were determined by XRF and XRD.The thermal events observed in the range from room temperature to 1300°C were related to the sample composition. The first mass loss step was related to free water content, while many of the other processes were related to dehydration processes. It was found that most of the decomposition reactions of hydrohematite, ferrihydrite, aluminogoethite, boehmite, silicates and carbonates were strongly overlapping. It was also explained the formation of silicates and calcium titanate, which presence was confirmed at 1000°C by XRD.

Keywords: *red mud, TG, thermal, XRD*

Introduction

The Bayer Process is the principal industrial means of producing alumina [1]. In general, red mud is the most abundant byproduct generated during the Bayer process for alumina production. It is the insoluble product after bauxite digestion with sodium hydroxide at elevated temperature and pressure. It is a mixture of compounds originally present in the parent mineral, bauxite, and of compounds formed or introduced during the Bayer cycle. Red mud is highly alkaline with a pH usually ranging from 10 to 13 [2–4]. The worldwide annual production is 70 million tones [5]. Its disposal remains an issue of great importance with environmental implications. The amount stored in Galicia–Spain is about 15 million tons, increasing at a rate of 1 million tons per year. It is mixed with some granite rocks in order to reduce its pH. The storage facility, consisting basically in a granite walled reservoir, will be full in the next couple of years. It could become an environmental since granite can theoretically react in highly alkaline media. A high number of potential uses has been reported, including metallurgical ones (iron and steel production, titania, alumina and alkali, minor constituents recovery), production of building materials (constructional brick, light weight aggregates, bricks roofing and flooring tiles, cements etc.), catalysis, ceramics (pottery, sanitary ware, special tiles and glasses, glazes, ferrites) and other miscellaneous direct uses (in waste treatment, as a filler, as a fertilizer, etc.). Red mud varies in chemical and physical properties depending primarily on the bauxite used and, to a lesser extent, the manner in which it is processed [6]. The amount of residue generated, per tonne of alumina produced varies greatly depending on the type of bauxite used, from 0.3 tonnes for high-grade bauxite to 2.5 tonnes for very low grade. Its application in acid soils was considered for agricultural uses, but some pH correction is needed due to its high alkalinity. The red slurry may also content heavy metals that could leak originating serious environmental problems. On the other hand, utilization of this product as an additional raw material for ceramic manufacturing seems to be possible. In principle, the heavy metals could be stabilized in a ceramic matrix. It is necessary to know the thermal behavior of this material in order to design any manufacturing process. Red muds from several sources have been studied by thermal analysis and other techniques [6–12]. The data reported show that some differences exist between them. No report was found about thermal characterization of the Spanish red mud.

Experimental

Red mud samples were collected from upper layer of the red mud outdoors stockpile of the Alcoa-San Ciprian Spanish factory. The sample stayed in the stockpile about six months.

Total element composition was analyzed by X-ray fluorescence spectroscopy (XRF). Mineral composition was determined by X-ray diffraction (XRD) at room temperature and at 1000°C. The samples were also used for simultaneous thermal analysis, thermogravimetric analysis (TG) and differential scanning calorimetry (DSC).

Simultaneous DSC and TG experiments were performed in a Rheometrics STA 1500. A purge of dry

* Author for correspondence: rartiaga@udc.es

1388–6150/$20.00

Akadémiai Kiadó, Budapest, Hungary
Springer, Dordrecht, The Netherlands

air at 50 mL min^{-1} was kept along all the experiments. The samples were placed in high alumina crucibles. A fresh sample of 31.41 mg was used for the first scan. The material resulting from the first scan, with a mass of 17.38 mg, was used as sample for a second experiment.

In both cases, the experimental setup consisted of a heating ramp from 25 to 1400°C at 20°C min^{-1}, followed by a cooling ramp from 1400°C to room temperature at 20°C min^{-1}. In order to remove the free water, a part of the red mud was dried at 70°C for 12 h in an oven. A sample of 17.30 mg of dried red mud was tested in the simultaneous instrument in the range from room temperature to 900°C. In order to improve the resolution a lower heating rate of 10°C min^{-1} was used in this case. The other setup parameters were the same than in the previous experiments.

Results and discussion

Chemical and mineralogical analysis

The pH of the sample was 11 and the density 2.0 g cm^3.

Tables 1 and 2 show, respectively, the mineral and chemical compositions of the Spanish–San Ciprián red mud along with data from the literature: pure Bayer Process Chinese–Pingguo red mud (PBPRM) [7], the

Table 1 Mineral composition of the Spanish red mud compared with data reported from other red muds. Presence is indicated by 'X'

Mineral composition	Spanish San Ciprián RM	Pingguo PBPRM [7]	Zhengzhou BPBCRM [6]	Cagliari RM [8]	Aughinish RM [9]	Seydisehir RM [9]
Hydrohematite $Fe_2O_3 \cdot xH_2O$	x					
Hematite α-Fe_2O_3	x	19	7	x	x	x
Aluminogoethite, 14% M of Al substitution	x					
Ferrihydrite $Fe_5O_7(OH) \cdot 4H_2O$	x					
Rutile TiO_2	x	3		x	x	
Calcite $CaCO_3$	x	12	42			
Boehmite AlO(OH)	x			x	x	x
Natrodavyne high form, $3NaAlSiO_4 \cdot Na_2CO_3$	x					
Plazolite, $Ca_3Al_2Si_2O_8(OH)_4$	x					
$Ca_3AlFe(SiO_4)(OH)_8$	x					
Sodium carbonate hydrate $Na_2CO_3 \cdot H_2O$	x					
Quartz SiO_2	small amount			x	x	
Amorphous	important amount	22	22			
Chantalite $CaAl_2SiO_4(OH)_4$				x		
Calcium aluminium silicate $Ca_2Al_2(SiO_4)(OH)_8$					x	x
Cancrinite $Na_6Ca_2Al_6Si_6O_{24}(CO_3)_2$				x		
$Na_5Al_3CSi_3O_{15}$				x		
Bayerite				x		
Anatase TiO_2				x		
Calcium silicates $CaSiO_3$					x	x
Imogolite $Al_2SiO_3(OH)_4$		32				
Ilmenite $FeTiO_3$		10				
Perovskite $CaTiO_3$			11		x	
$Illite(K,H_3O)(Al,Mg,Fe)_2(Si,Al)_4O_{10}[(OH)_2,(H_2O)]$			7			
Magnetite Fe_3O_4			5			
Sodalite $Na_2O \cdot Al_2O_3 \cdot SiO_2$					x	x
Goethite FeO(OH)					x	x
Gibbsite $Al_2O_3 \cdot 3H_2O$				x	x	x

Table 2 Chemical composition of the Spanish red mud and data reported from other red muds. The values are given in mass percent, except when ppm is indicated

	Spanish RM	Pingguo PBPRM [7]	Zhengzhou BPBCRM [6]	Cagliari RM [8]	Aughinish RM [9]	Seydisehir RM [9]	Hungarian RM [12]	German RM [12]	Sicilian RM [12]	IAI [13]
Fe_2O_3	47.85	26.9	12.5	35.2	30.4	39.84	37.08	43.94	46.12	30–60
Al_2O_3	20.20	26.8		20.0	23.6	20.24	13.64	14.08	15.34	10–20
SiO_2	7.50	13.1	19.9	11.6	9.65	15.24	12.41	10.34	8.32	3–50
TiO_2	9.91	7.3	6.7	9.2	17.85	4.15	3.50	7.27	8.82	trace-10
Na_2O	8.40		2.4	7.5	5.3	9.43	8.76	8.15	6.36	2–10
CaO	6.22	23.5	41.6	6.7	6.4	1.80	9.37	4.36	4.39	2–8
MgO	0.33	1.1	1.0	0.4			1.01	0.67	0.38	
Cr_2O_3		0.5		0.4						
Cr	ND						0.059	0.158	0.056	
ZrO_2		0.5		0.3						
CO_2			5.9							
K_2O	0.11		0.8				0.37	0.36	0.02	
P_2O_5	0.46			0.3			0.08	0.11	0.20	
SO_3				0.3						
S	636 ppm						0.55	0.23	0.12	
Cl	ND			0.2						
MnO	0.07									
MnO_2							0.94	0.08	0.05	
Dy (ppm)	5									
Er (ppm)	5									
Eu (ppm)	4									
F (ppm)	7142									
Gd (ppm)	12									
Pr (ppm)	19									
Tb (ppm)	2									
V	ND						0.134	0.17	0.086	
Other				0.6	6.8	0.48				
Loss on ignition at 900°C				7.3						
Loss on ignition at 1050°C							9.57	9.65	9.61	

combined Bayer Process and bauxite calcination Chinese–Zhengzhou red mud (BPBCRM) [6], Italian–Cagliari [8], Irish–Aughinish and Turkish–Seydisehir [9] red muds.

Table 2 also includes the main constituents of Hungarian, German and Italian–Sicilian [12] red muds and the variation reported by the International Aluminium Institute [13]. The mineral phases observed at 1000°C are hematite, calcium and iron titanate ($Ca_4Fe_2Ti_2O_{11}$), carnegieite alpha ($NaAlSiO_4$) and a calcium titanate ($CaTiO_3$) perovskite.

It is clear from Table 1 that several varieties of red mud can exist, containing many mineralogical phases. The differences between these different varieties of red mud are due to the type of bauxite used and to the

Bayer process parameters, such as temperature and pressure, amount of caustic soda added, etc.

The following elements were not detected by XRF in the Spanish red mud: As, Ba, Ce, Cl, Co, Cs, Cu, Ga, Hf, La, Lu, Mo, Nb, Ni, Pb, Rb, Sb, Sc, Sn, Sr, Ta, Th, Tl, Tm, U, W, Y, Yb and Zn.

It can be seen from Table 2 that the content of the Spanish red mud in Fe_2O_3, TiO_2 and F is higher than in most of the cases reported in the literature. The two first compounds are interesting for industrial applications due to their ability to tune the color of ceramics by adjusting the red mud content and the processing conditions.

The presence of SiO_2 is also interesting since its reaction with Na_2O, K_2O and CaO present can lead to compounds with lower melting temperature than the other components of the sample. It would provide for a liquid phase in the grain boundaries, facilitating the sintering of these materials.

Thermal analysis

Figure 1 shows an overlay of the TG curves obtained from an as received industrial waste sample and a dried one. It can be observed that the first mass loss step of the fresh sample is mostly due to free water evaporation. The mass loss observed in the dry sample from the beginning up to 200°C can be attributed to hydrohematite dehydration [14] and the first step of ferrihydrite dehydration [15] and represents 1.9%. The free water content of the fresh sample was determined from the first mass loss step of the fresh sample curve by subtraction of the mass loss observed in the same range of temperature on the dry sample curve. It represents about 33.3% of free water content.

Figure 2 shows the DSC, TG and the first derivative of the TG with respect to the time (DTG) curves obtained from the fresh sample during the heating ramp. It can be observed that the main mass loss processes end at around 600°C, although a very slow mass loss process continues up to the end of the experiment.

The first mass loss process appears as a peak at 136.19°C on the DTG curve, which reaches a zero value at 246°C. It is associated with an endothermic peak on the DSC trace and can be attributed to water evaporation, 'weakly bound' water removable from hydrohematite [14, 16, 17] and ferrihydrite dehydration [15]. Two parts can be observed in this peak. The maximum slope of the curve is reached at around 150°C. In evaporation processes, it is typical that the DTG curve reaches its maximum slope at the end of the process [18]. As explained for Fig. 1, the peak area below 150°C is mostly due to water evaporation.

The range from 150 to 246°C can be assigned to hydrohematite [14] and ferrihydrite [15] dehydration and represents 1.39% of the mass sample.

There is a small endothermic peak at around 283°C and other bigger at around 347°C. The last one is accompanied by an important mass loss. The both peaks can be attributed to Al-goethite dehydroxylation and can be interpreted by the difference in the dehydroxylation temperatures of Al–OH and Fe–OH groups [19]. In the literature, the double peak was attributed to an intermediate goethite with a slightly higher dehydroxylation temperature generated during heating [20]. Other authors suggested that the hematite shell formed around goethite crystals retards the dehydration of the core [21]. It was reported that the lower the particle size of the sample, the narrower the dehydroxylation peaks. For enough small particles a single peak may appear [22]. Other authors mentioned a single peak [10, 23]. It was also found that the temperature of dehydroxylation maximum obtained from DTG curves rose with increasing Al-substitution [24].

As can be observed in Fig. 3, in a more convenient scale, the peak at 347°C, on the DTG curve, is followed by a long tail that expands to 600°C and is accompanied by two small endothermic peaks, on the DSC curve, at 475 and 535°C. The shape of the DTG curve, along that region, indicates that several mass loss processes overlap strongly. The first portion of this region is

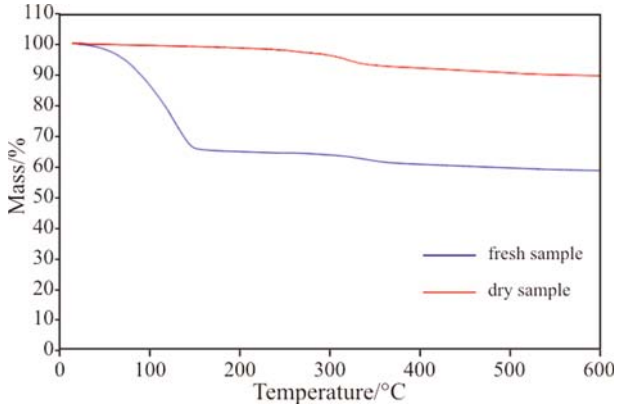

Fig. 1 Overlay of the TG traces obtained from a wet and a dry red mud samples

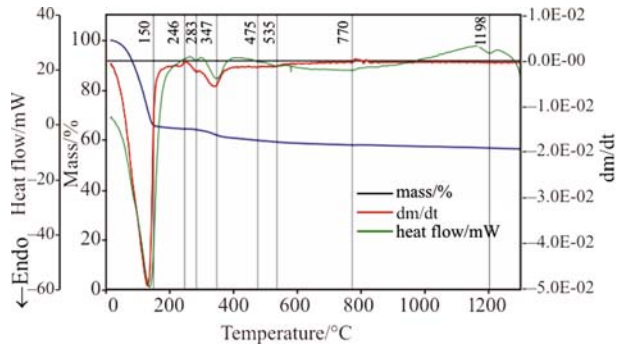

Fig. 2 DSC, TG and DTG curves obtained from the first heating scan of a fresh red mud sample

probably mostly due to the silicates dehydroxylation. The next part, accompanied by the 475°C peak can be assigned to boehmite decomposition [9, 23]. The range around the 535°C endothermic peak can be assigned to the second part of ferrihydrite decomposition [15].

The DSC trace in Fig. 2 shows that at 580°C begins an endothermic effect that ends around 1100°C. Taking into account the initial composition of the sample, it is likely that around 580°C begins the following endothermic reaction [25]:

$$Na_2CO_3+CaCO_3 \rightarrow Na_2Ca(CO_3)_2$$

At 680°C this compound can start to react with the silica present in the sample producing the following substances: $2[Na_2O{\cdot}2SiO_2]+[Na_2O{\cdot}3CaO{\cdot}6SiO_2]$, what is also an endothermic process associated with mass loss [25]. This process was reported to end at 830°C [26–28].

In the range from 600 to 800°C, it is also likely that it takes place the formation of $Na_2SiO_3+CaSiO_3$.

The endothermic peak observed at 770°C is probably due to peritectic melting of calcium disilicate, which can react in liquid phase [25]:

$$[Na_2O{\cdot}3CaO{\cdot}6SiO_2]+[Na_2O{\cdot}2SiO_2] \rightarrow$$
$$\rightarrow [Na_2O{\cdot}2CaO{\cdot}3SiO_2]+\text{líquidus}$$

It was reported that calcium carbonate decomposition takes place between 680 and 776°C [11], and, in the case of other red muds, between 560 and 720°C [6]. The calcium carbonate present in the sample is expected to decompose in this range of temperature. The CaO resulting from the calcium carbonate decomposition may react with titanium oxide [25]:

$$CaO+TiO_2 \rightarrow CaTiO_3$$

This reaction was confirmed by the presence of calcium titanate at 1000°C, which was not present in the original sample. The reaction of formation of $CaTiO_3$ from CaO and TiO_2 is exothermic, but there is no exothermic peak on the DSC curve that can confirm that this reaction occurred. The exothermic peak on DSC curves is probably hidden under the endothermic peak of $CaCO_3$.

Silicates formation was also reported for the range from 600 to 1000°C, overlapping with the calcium carbonate decomposition [25]:

$$Na_2CO_3+SiO_2 \rightarrow Na_2SiO_3+CO_2(g)$$

$$2CaCO_3+SiO_2 \rightarrow Ca_2SiO_4+2CO_2(g)$$

$$Ca_2SiO_4+SiO_2 \rightarrow 2CaSiO_3$$

Other process that can be responsible of the very slow mass change that continues at temperature above 600°C is the residual hydrohematite dehydration. Only part of hydrohematite dehydrates at 160–200°C [29].

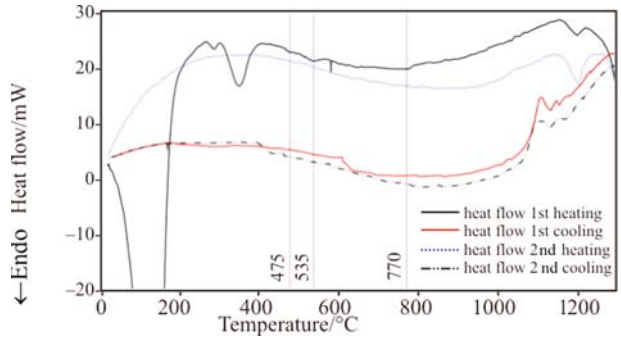

Fig. 3 Overlay of the heat flow plots obtained from a fresh red mud sample in the first heating experiment, first cooling, second heating and second cooling

It was reported that small quantities of water in this species resist heating even at 1000°C [16].

There is an endothermic peak at 1198°C that can be attributed to melting of some of the silicates present at that temperature.

Figure 3 plots an overlay of the heat flow plots obtained during the first and second heating-cooling cycles. The sample mass did not change after completion of the first heating scan. It means that no dehydration or decomposition occurred beyond the first heating scan. The first cooling DSC trace shows an exothermic peak at around 1100°C. It is compatible with some crystallization processes. The second heating and cooling ramps gave again these peaks. It confirms the hypothesis of melting at 1198°C during the heating ramp and crystallization during the cooling ramp at 1100°C in a crystalline form. No other noticeable thermal events were found.

Conclusions

Chemical and mineralogical composition of a Spanish red mud was determined by XRF and XRD. Several thermal events were observed by simultaneous TGA-DSC in the range from room temperature to 1400°C and were related to the composition of the sample. Decomposition reactions of hydrohematite, ferrihydrite, aluminogoethite, boehmite, silicates and carbonates were located on the TG curve. Most of the processes were strongly overlapping. It was also found formation of silicates and calcium titanate, which presence was confirmed at 1000°C by XRD.

Acknowledgements

The 5th author gratefully acknowledge support from the Spanish Ministerio de Educacion y Ciencia (MTM2005-00429).

References

1 A. R. Hind, S. K. Bhargava and S. C. Grocott, Colloids Surf. A, Physicochem. Eng. Aspects, 146 (1999) 359.
2 N. W. Menzies, I. M. Fulton and W. J. Morrell, J. Environ. Qual., 33 (2004) 1877.
3 C. Lin, G. Maddocks, J. Lin, G. Lancaster and C. Chu, Aust. J. Soil Res., 42 (2004) 649.
4 R. N. Summers and J. D. Pech, Agr. Ecosyst. Environ., 64 (1997) 219.
5 Red Mud Project: red mud information. (2008). Retrieved 13 May, 2008, from University of Coruña. Web site: http://www.redmud.org/home.html.
6 Y. Liu, C. Lin and Y. Wu, J. Hazard Mater., 146 (2007) 255.
7 C. Lin, Bauxite residue (red mud) from the Pingguo alumina refined, China: characteristics and potential uses. In A. G. Pasamehmtoglu, A. Ozgenoglu and A. Y. Yesilay (ed.) Proceedings of International Symposium on Environmental Issues and Waste Management in Energy and Mineral Production, Atilim University, Turkey (2004) 551.
8 V. M. Sglavo, R. Campostrini, S. Maurina, G. Carturan, M. Monagheddu, G. Budroni and G. Cocco, J. Eur. Ceram. Soc., 20 (2000) 235.
9 A. Atasoy, J. Therm. Anal. Cal., 90 (2007) 153.
10 A. Atasoy. J. Therm. Anal. Cal., 81 (2005) 357.
11 A. Alp and M. S. Gora. J. Therm. Anal. Cal., 73 (2003) 201.
12 T. Egyházy, J. Kovács, T. Fülöp and K. Solymár, Utilisation of bauxite residue by modified metallurgical concept. In Travaux, Környezetmérnöki és Kémiai Technológia Intézeti Tanszék (2004) 77–85.
13 International Aluminium Institute. Sustainability. Bauxite residue (2008). Retrieved 13 May, 2008, from University of Coruña. Web site: http://www.world-aluminium.org/Sustainability/Environmental+Issues/Bauxite+residue
14 M. M. Gasik and M. I. Gasik, Smelting of Aluminum. In G. E. Totten, D. Scott MacKenzie (Ed.) Handbook of Aluminum, Vo.l 2: Alloy Production and Materials, CRC Press, (2003) p. 50.
15 I. Mitov, D. Paneva and B. Kunev, Thermochim. Acta, 386 (2002) 179.
16 E. Wolska, Z. Kristallogr., 154 (1981) 69.
17 A. A. Kavanov, Russ. J. Appl. Chem., 76 (2003) 1045.
18 J. H. Suwardie, R. Artiaga and F. Barbadillo, Thermochim. Acta, 392 (2002) 289.
19 M. B. Fey and J. B. Dixon, Clays Clay Miner., 29 (1981) 91.
20 U. Schwertmann, Thermochim. Acta, 78 (1984) 39.
21 R. Derie, M. Ghodsi and C. Calvoroche, J. Thermal Anal, 9 (1976) 435.
22 D. Walter, G. Buxbaum and W. Laqua, J. Therm. Anal. Cal., 63 (2001) 733.
23 M. Laskou, Margomenou-Leonidopoulou, G.. Balek, V., J. Therm. Anal. Cal., 84 (2006) 141.
24 H. D. Ruan and R. J. Gilkes, J. Thermal Anal., 46 (1996), 1223.
25 R. Jordán, T. Faria, G. Rodríguez, G. César-Díaz and M. E. Zayas, Ingeniería y Ciencía, 3 (2007) 91.
26 W. C. La Course, The Glass Researcher, 10 (2001) 18.
27 R. Brüning and M. Sutton, J. Non-Crystalline Solids, 205 (1996) 480.
28 T. L. Webb and H. Heystek, The carbonate minerals. In: R. C. Mackenzie, Editor, The Differential Thermal Investigation of Clays, Mineralogical Society, London (1957) pp. 329–363.
29 N. S. Kurnakow and E. J. Rode, Zeitschrift für anorganische und allgemeine Chemie, 169 (1928) 57.

Received: May 14, 2008
Accepted: July 15, 2008
Online First: November 11, 2008

DOI: 10.1007/s10973-008-9230-9